edx lu_879 report (2025/04)

David Lu

Abstract

This report describes the design, simulation and analyse of Mach-Zehnder interferometer using a square waveguide in order to decrease at much as possible the variation between TE and TM polarisation, using Ansys Lumerical simulation tools. In a second phase, the device will be manufactured through electro-beam lithography technology. Then we will be able to compare the simulation with the manufactured device and evaluate the stability of the fabrication process.

1 Introduction

The main goal of this course is to learn how to design, characterize and evaluate the limitations of PIC devices. Working in telecommunication, I would like to introduce this technology into our company. I also evaluate the possibility of using Ansys Lumerical for simulation and design. This first touch with those tools will help me determine how easy we can introduce this tool into our company.

2 Theory

MZI is an optical device with at least two ports which can have many applications in optics since its functionalities are versatile. Depending on the design, we can choose different functionalities such as:

- Couplers
- Filters
- Amplitude or Phase modulators
- Sensing applications
- Etc.

Basically, MZI can be designed with two beam combiners and two waveguides. Figure 1 is one example of MZI design. One of the combiners will separate an external optical signal. Both signals will travel through separate waveguides and then will be recombined through the second combiner.

The two waves traveling through separate waveguides will go through different external elements such as mechanical thermal or even electrical stress which could change the phase of the signal. Output signal will then be a combination of the two separate waveguides and its response is described in the equation below.

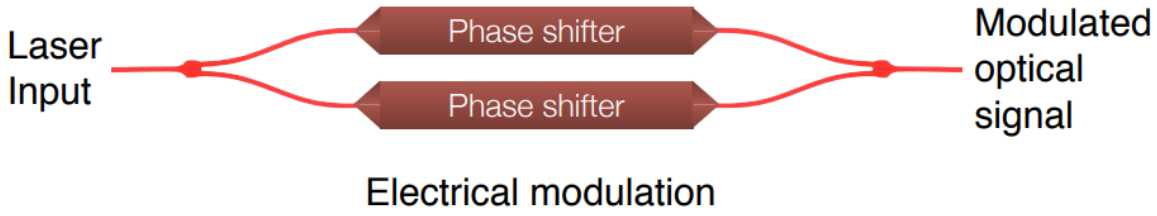

Figure 1: MZI in a balanced configuration. Both branches have the same length L, effective index neff and propagation loss.

By considering the input electrical field $\boldsymbol{E_i}$ which is equally separated by $\boldsymbol{E_{i1}}$ and $\boldsymbol{E_{i2}}$ we have the following equation:

$$E_{i1} = \mathbf{E_{i2}} = \frac{\boldsymbol{E_i}}{\sqrt{\mathbf{2}}}$$

With $I_1 = I_2 = \frac{I_i}{2}$ and $I_i = |E|^2$

When recombining $\boldsymbol{E_{i1}}$ and $\boldsymbol{E_{i2}}$ to get $\boldsymbol{E_o}$ the output electrical field we have the following equation:

$$\boldsymbol{E_o} = \frac{\boldsymbol{E_i}}{\mathbf{2}}(\boldsymbol{e}^{-i\beta_1 L_1 - \frac{\alpha_1}{2}L_1} + \boldsymbol{e}^{-i\beta_2 L_2 - \frac{\alpha_2}{2}L_2})$$

Then the intensity is:

$$\boldsymbol{I_0} = \frac{\boldsymbol{I_i}}{\mathbf{4}}\left|\boldsymbol{e}^{-i\beta_1 L_1 - \frac{\alpha_1}{2}L_1} + \boldsymbol{e}^{-i\beta_2 L_2 - \frac{\alpha_2}{2}L_2}\right|^2$$

If we neglect the attenuation of the waveguides $\boldsymbol{\alpha_1 = \alpha_2 = 0}$ and introduce Euler's and trigonometric formulas, we can simplify the expression to:

$$\boldsymbol{I_0} = \frac{\boldsymbol{I_i}}{\mathbf{2}}[\mathbf{1} + \boldsymbol{cos}(\boldsymbol{\beta_1 L_1 - \beta_2 L_2})]$$

By considering that the effective index $n_1 = n_2$, we then have two cases.

1) a balanced interferometer represented by the following equation:

$$\boldsymbol{I_0 = I_i}$$

2) an imbalanced interferometer represented by the following equation:

$$\boldsymbol{I_0} = \frac{\boldsymbol{I_i}}{\mathbf{2}}[\mathbf{1} + \boldsymbol{cos}(\boldsymbol{\beta \Delta L})]$$

Then by following the method described in Silicon Photonics Design book [1] we can determine the FSR expression in Hz:

$$FSR = \Delta v = \frac{c}{\Delta L(n + v\frac{dn}{dv})} = \frac{c}{\Delta L n_g} = [Hz]$$

We can also approximate the FSR in m:

$$FSR = \Delta\lambda \approx \frac{\lambda^2 \Delta v}{c} = \frac{\lambda^2}{\Delta L n_g} = [m]$$

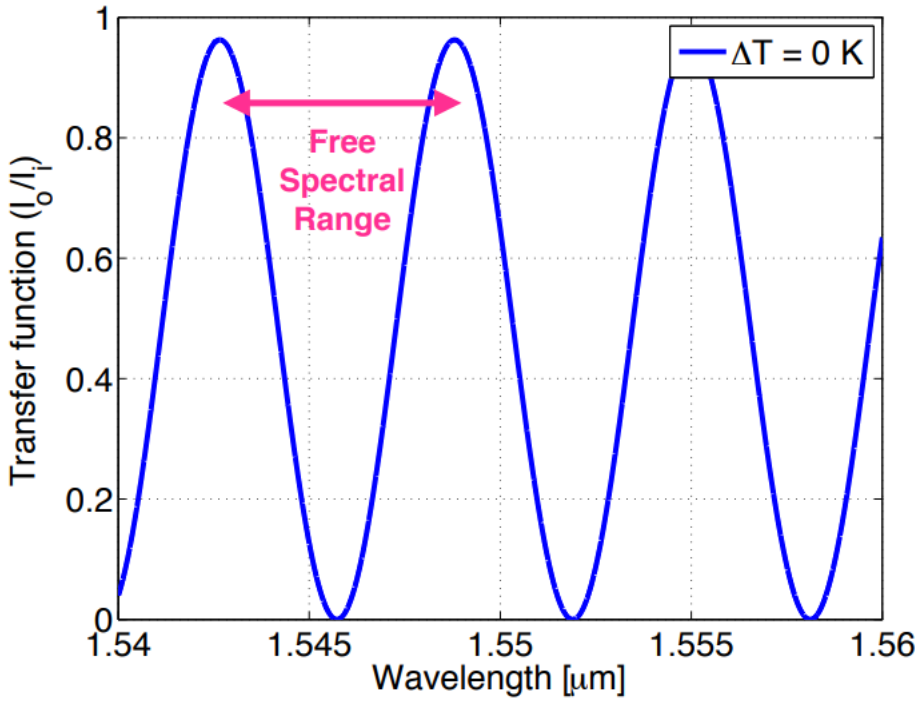

Figure 2 : FSR definition

3 Modelling and Simulation

In this report we will design, simulate, characterize and analyze an imbalance MZI with a strip waveguide with 220nm width and 220nm height, with a $\Delta L = 100\mu m$. The study is focused on evaluating the performance of a square waveguide to have a system with both TE and TM polarization.

With Lumerical MODE [2] we can plot the TE and TM field intensity as represented in Figure 3 and Figure 4.

We can also have a look at the energy density of TE and TM as represented in Figure 5 and Figure 6.

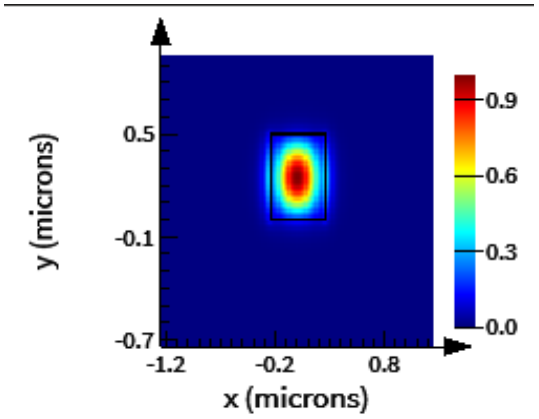

Figure 3 : TE polarization field in square waveguide

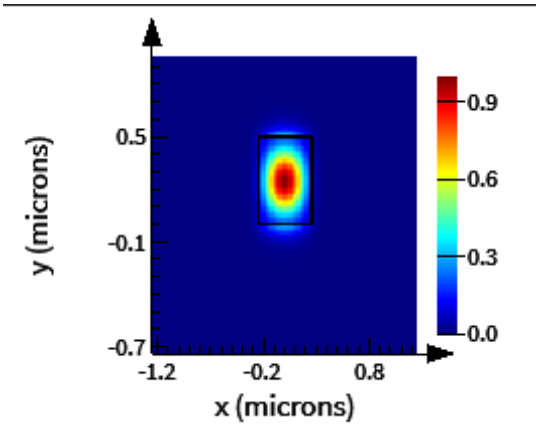

Figure 4 : TM polarization field in square waveguide

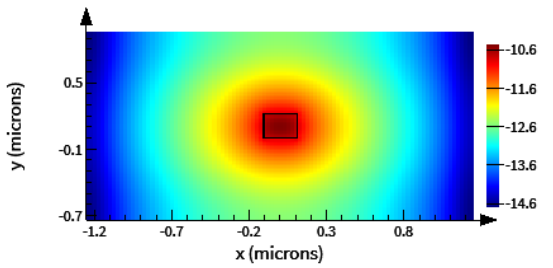

Figure 5 : TE polarization energy density in square waveguide

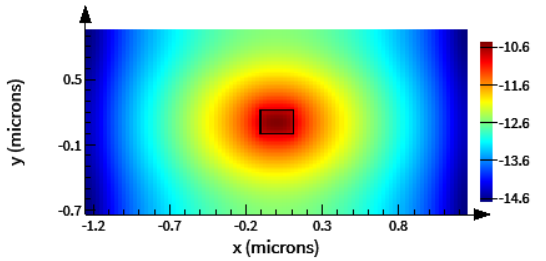

Figure 6 : TM polarization energy density in square waveguide

We can also plot the effective index and the group index of the waveguide versus wavelength of TE (in blue) and TM (in green) using Lumerical Mode.

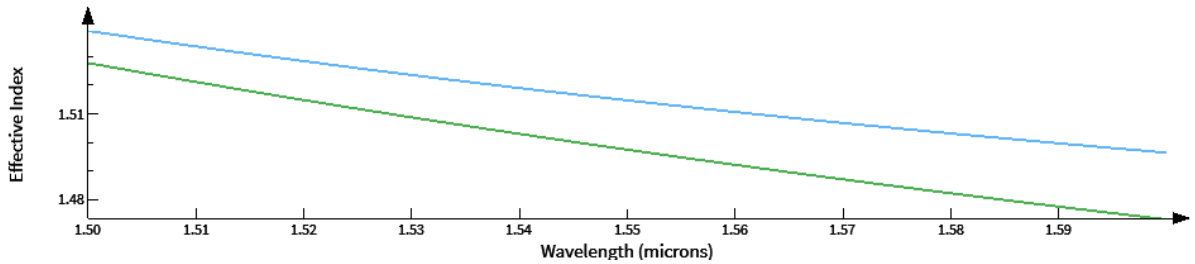

Figure 7 : Effective index vs wavelength of TE and TM

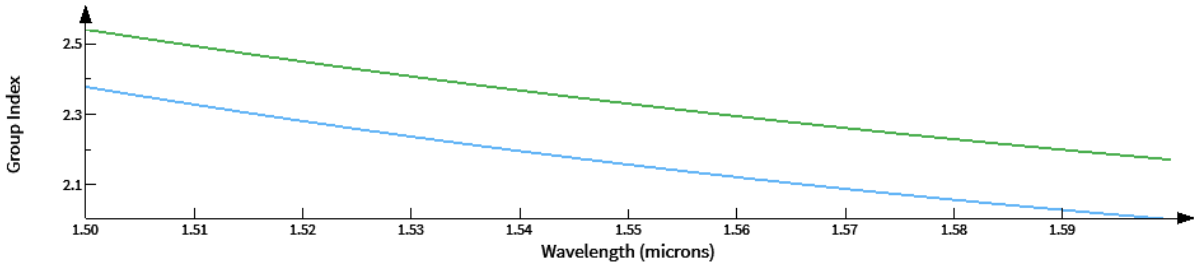

Figure 8 : Group index vs wavelength of TE and TM

Also using the compact model of the waveguide with Lumerical mode script, the effective index at 1550nm is as follow:

$$n_{eff} = 1.51 - 1.50(\lambda - \lambda_0) - 0.42(\lambda - \lambda_0)^2$$

Then we use Lumerical Interconnect [2] to create the MZI system (see Figure 9) and use and ONA to mesure the transfer fonction of this system (see Figure 10).

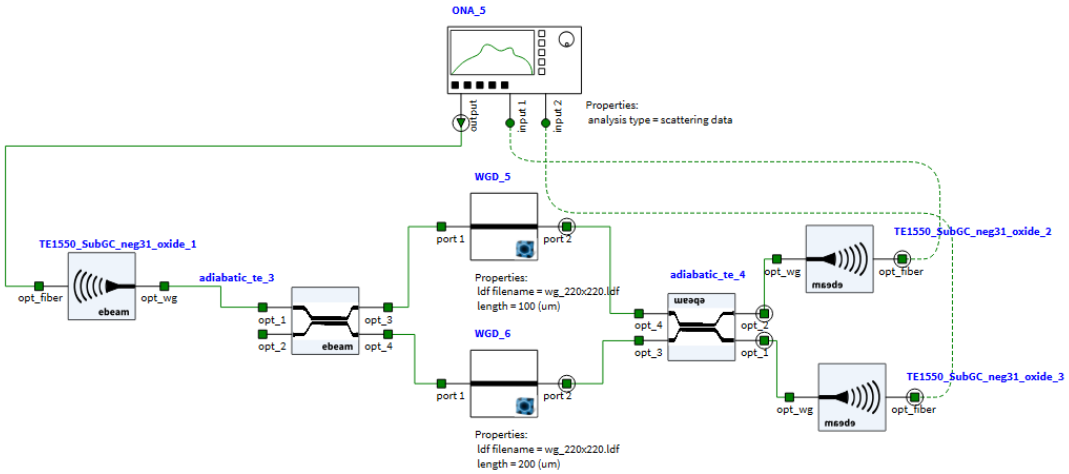

Figure 9 : MZI model using square waveguide. This setup allows to measure TE only. TM setup is the same but with TM grating couplers, beam combiners and ONA configuration to measure TM.

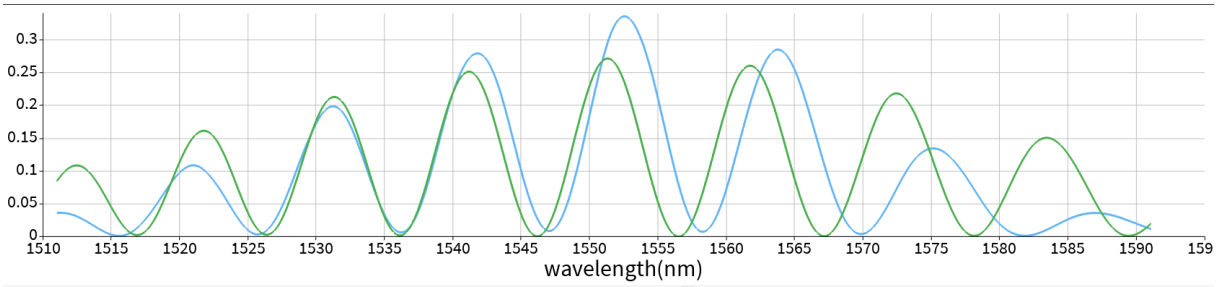

Figure 10 : MZI transfer function of TE in blue and TM in green

We can see several artifacts on the transfer function such as dependance to wavelength and different FSR and low transmission (below 35%).

We can try to understand where the issue comes from by simulating the different elements of the setup separately. First we simulate the waveguide in Figure 11, then two grating couplers in Figure 12 and finally two adiabatic couplers in Figure 13.

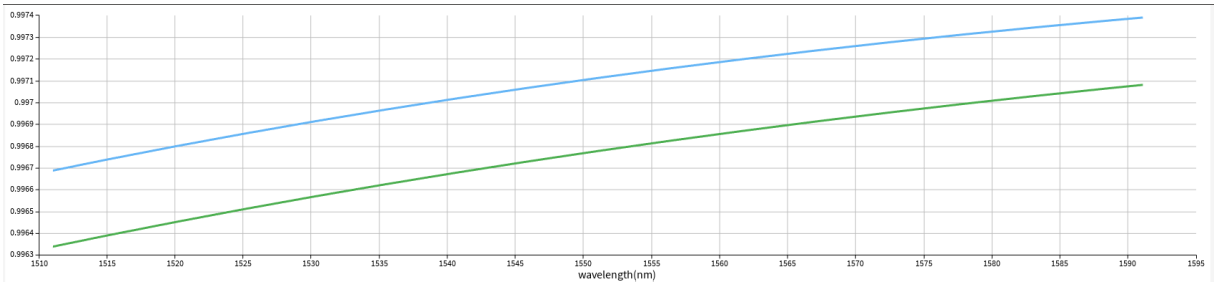

Figure 11 : Square waveguide 220x220nm transfer function of TE in blue and TM in green

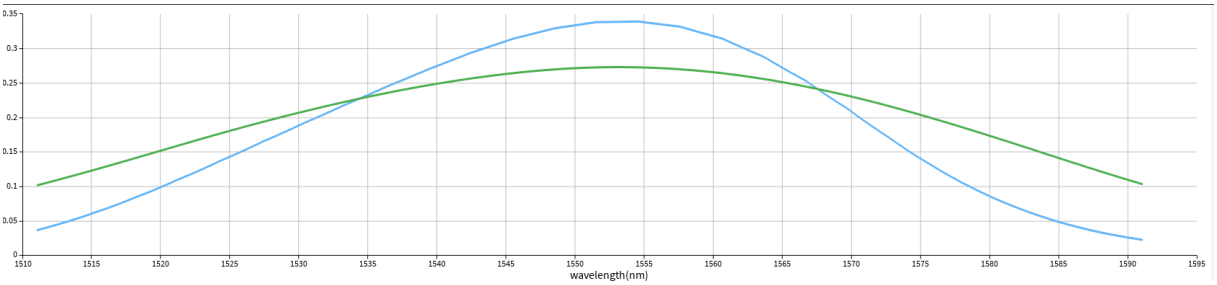

Figure 12 : Two Grating couplers transfer function TE in blue and TM in green

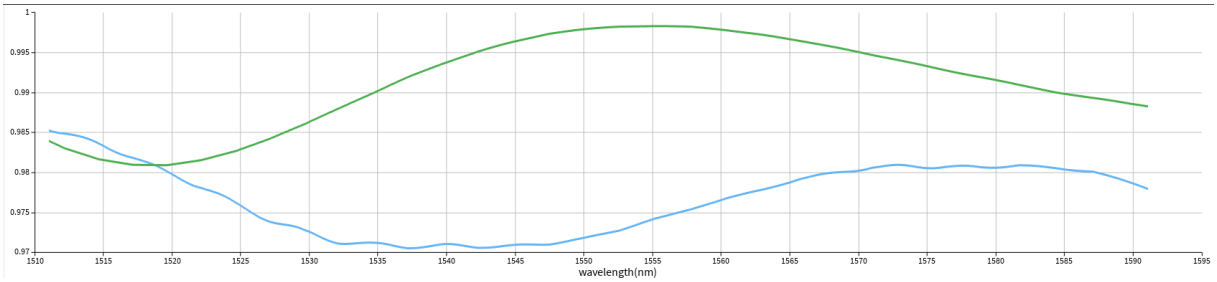

Figure 13 : Two adiabatic couplers transfer function TE in blue and TM in green

We can see on that waveguide and the couplers are sightly sensitive to wavelength but the most sensitive is the grating couplers as expected.

For the waveguide, TE and TM transfer functions are similar with a neglectable offset (less than 1%).

For the grating and adiabatic couplers TE and TM transfer functions are not neglectable which results in an amplitude variation on the total transfer function of Figure 10.

We also must note that despite the $\boldsymbol{\Delta L}$ equal for TE and TM simulation, the FSR are still different. By looking at the FSR formula again, we can suppose that the main variation comes from the $\boldsymbol{n_g}$.

$$\boldsymbol{FSR \approx \frac{\lambda^2}{\Delta L n_g}}$$

By simulating again in Lumerical Mode at 1550nm we the group index are $n_{gTE} = 2.16$ and $n_{gTM} = 2.33$. Then the FSR are:

$$\boldsymbol{FSR_{TE} \approx 11.1\ nm}$$

Whereas:

$$FSR_{TM} \approx 10.3\ nm$$

All those effects combined could explain the different transfer functions of the MZI. Now the goal would be to manufacture the same device several times in order to know the quality of the process of fabrication which will surely lead to a variation of ΔL and n_g which will lead to a dispersion of the FSR.

4 Fabrication

4.1 Layout

For the layout drawing, we use Klayout. We draw TE and TM MZI (with ΔL = 100µm) two times to evaluate the stability of manufacturing process.

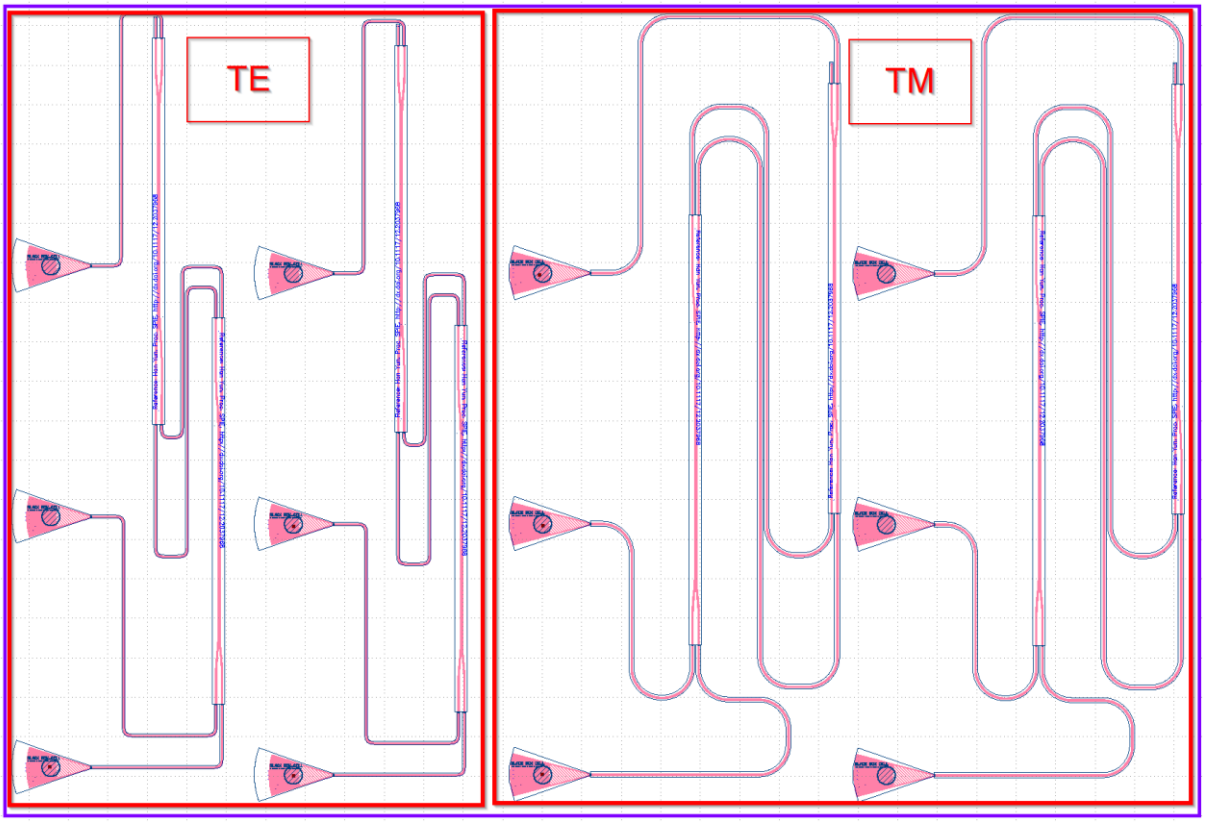

Figure 14 : Fabrication layout on Klayout

4.2 Applied Nanotools, Inc. NanoSOI process:

The photonic devices were fabricated using the NanoSOI MPW fabrication process by Applied Nanotools Inc. (http://www.appliednt.com/nanosoi; Edmonton, Canada) which is based on direct-write 100 keV electron beam lithography technology. Silicon-on-insulator wafers of 200 mm diameter, 220 nm device thickness and 2 µm buffer oxide

thickness is used as the base material for the fabrication. The wafer was pre-diced into square substrates with dimensions of 25x25 mm, and lines were scribed into the substrate backsides to facilitate easy separation into smaller chips once fabrication was complete. After an initial wafer clean using piranha solution (3:1 H2SO4:H2O2) for 15 minutes and water/IPA rinse, hydrogen silsesquioxane (HSQ) resist was spin-coated onto the substrate and heated to evaporate the solvent. The photonic devices were patterned using a JEOL JBX-8100FS electron beam instrument at The University of British Columbia. The exposure dosage of the design was corrected for proximity effects that result from the backscatter of electrons from exposure of nearby features. Shape writing order was optimized for efficient patterning and minimal beam drift. After the e-beam exposure and subsequent development with a tetramethylammonium sulfate (TMAH) solution, the devices were inspected optically for residues and/or defects. The chips were then mounted on a 4" handle wafer and underwent an anisotropic ICP-RIE etch process using chlorine after qualification of the etch rate. The resist was removed from the surface of the devices using a 10:1 buffer oxide wet etch, and the devices were inspected using a scanning electron microscope (SEM) to verify patterning and etch quality. A 2.2 µm oxide cladding was deposited using a plasma-enhanced chemical vapor deposition (PECVD) process based on tetraethyl orthosilicate (TEOS) at 300ºC. Reflectometry measurements were performed throughout the process to verify the device layer, buffer oxide and cladding thicknesses before delivery.

4.3 Manufacturing process

Due to the manufacturing process which can cause variability on width (caused by the waifer dimension) and height of the waveguide (EBL process), hence the effective index and group index will vary consequently. Here, we have a SOI wafers (UNIBOND) provided by Soitec, Grenoble, France.

The wafer lot we are using has the following parameters:

- 6" wafers, prime grade.
- Si thickness, mean = 219.2 nm
- Si thickness, 6 sigma = 23.4 nm (or +/- 3.9 nm, for one standard deviation)
- SiO2 thickness, mean = 2994.5 nm
- SiO2 thickness, 6 sigma = 6.3 nm

With that precious information we can perform a corner analysis and determine the effective index and group index of our waveguide using Ansys Mode. For this analysis we decided to not consider the variability of the EBL process due to lack of information and use 220 nm height.

From Figure 15 to Figure 18 we perform the corner analysis of the waveguide 220x220nm with width which varies from 195.8 to 242.6nm.

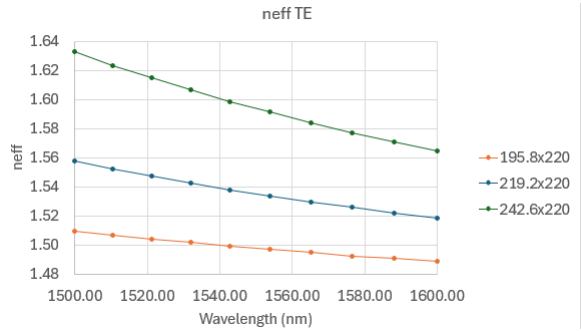

Figure 15 : effective index VS wavelength for TE

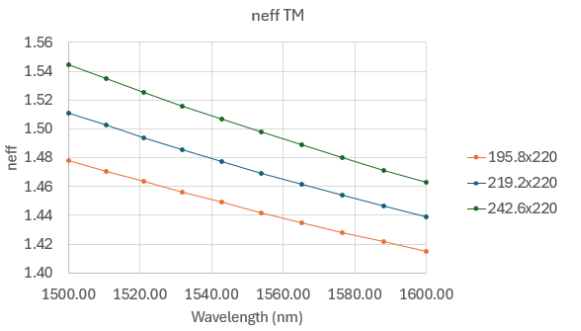

Figure 16 : effective index VS wavelength for TM

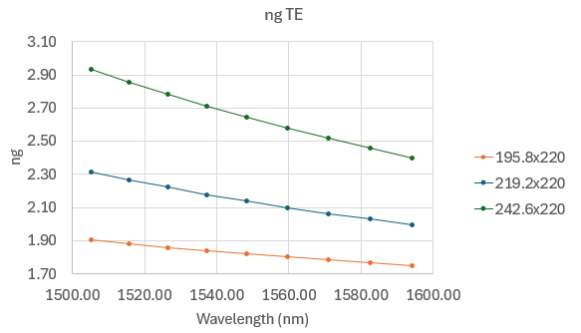

Figure 17 : group index VS wavelength for TE

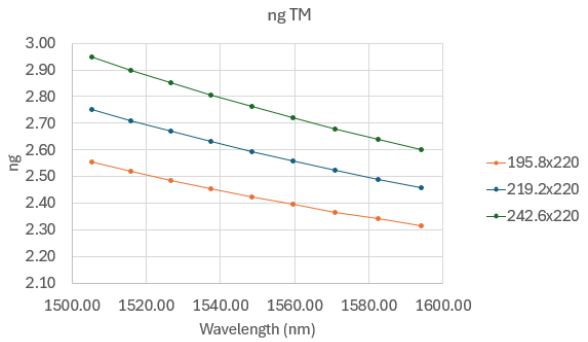

Figure 18 : group index VS wavelength for TM

4.4 Measurement description

To characterise the devices, a custom-built automated test setup [1] [3] [4] [5] [6] with automated control software written in Python was used [3]. An Agilent 81600B tunable laser was used as the input source and Agilent 81635A optical power sensors as the output detectors. The wavelength was swept from 1500 to 1600 nm in 10 pm steps. A polarization maintaining (PM) fibre was used to maintain the polarization state of the light, to couple the TE polarization into the grating couplers [4]. A 90° rotation was used to inject light into the TM grating couplers [4]. A polarization maintaining fibre array was used to couple light in/out of the chip [5].

5 Experiment data

One problem with the measurement data is that the grating couplers have a limited bandwidth. One way to remove the wavelength dependency loss of the grating couplers is to fit the curve with low order polynomial (order 4). The fitted curve is then removed from the raw data curve to get the final spectrum representing the transfer function of MZI as represented in Figure 19 and Figure 20 respectively for TE and TM.

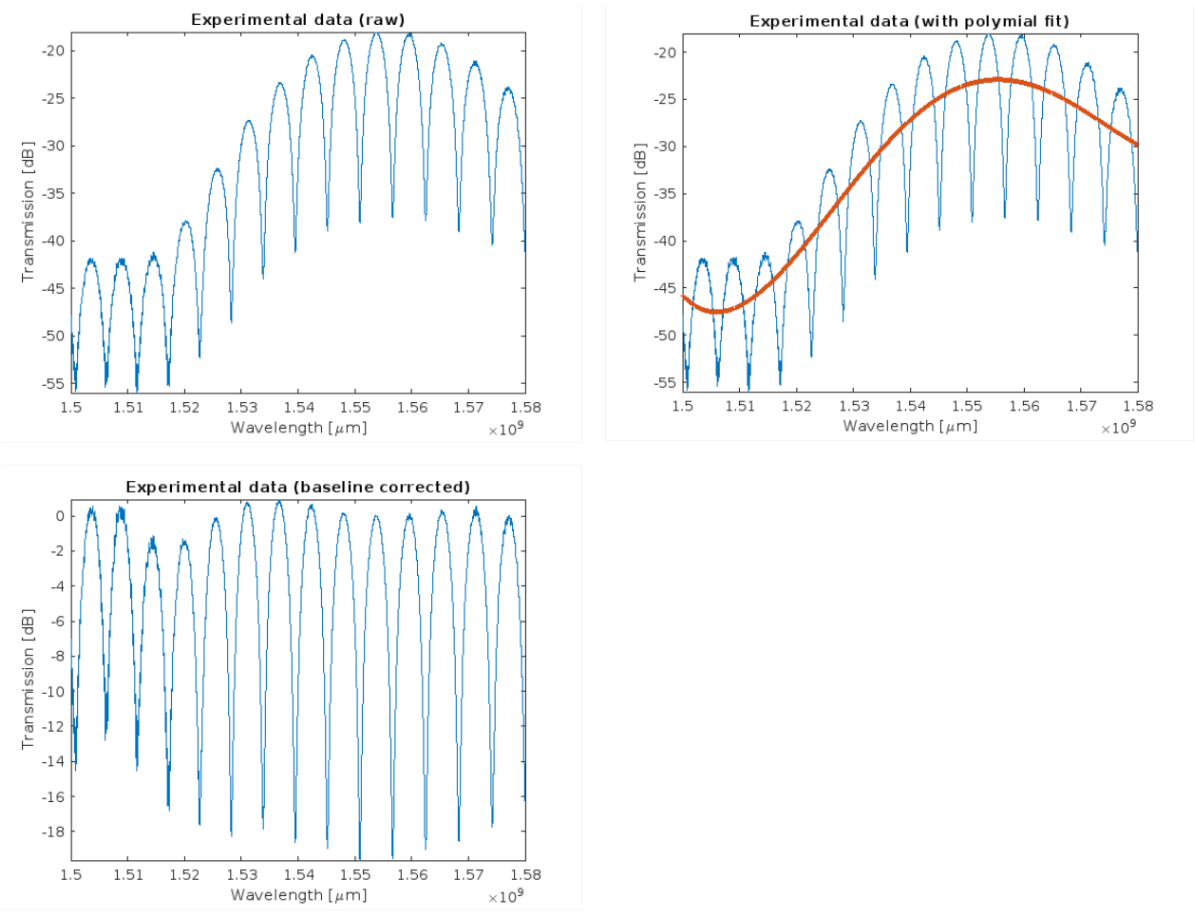

Figure 19 : TE1 Process of removing the grating couplers contribution on transmission spectrum. 1) Raw data. 2) Baseline curve in red representing grating couplers contribution. 3) Final spectrum with only MZI transmission spectrum.

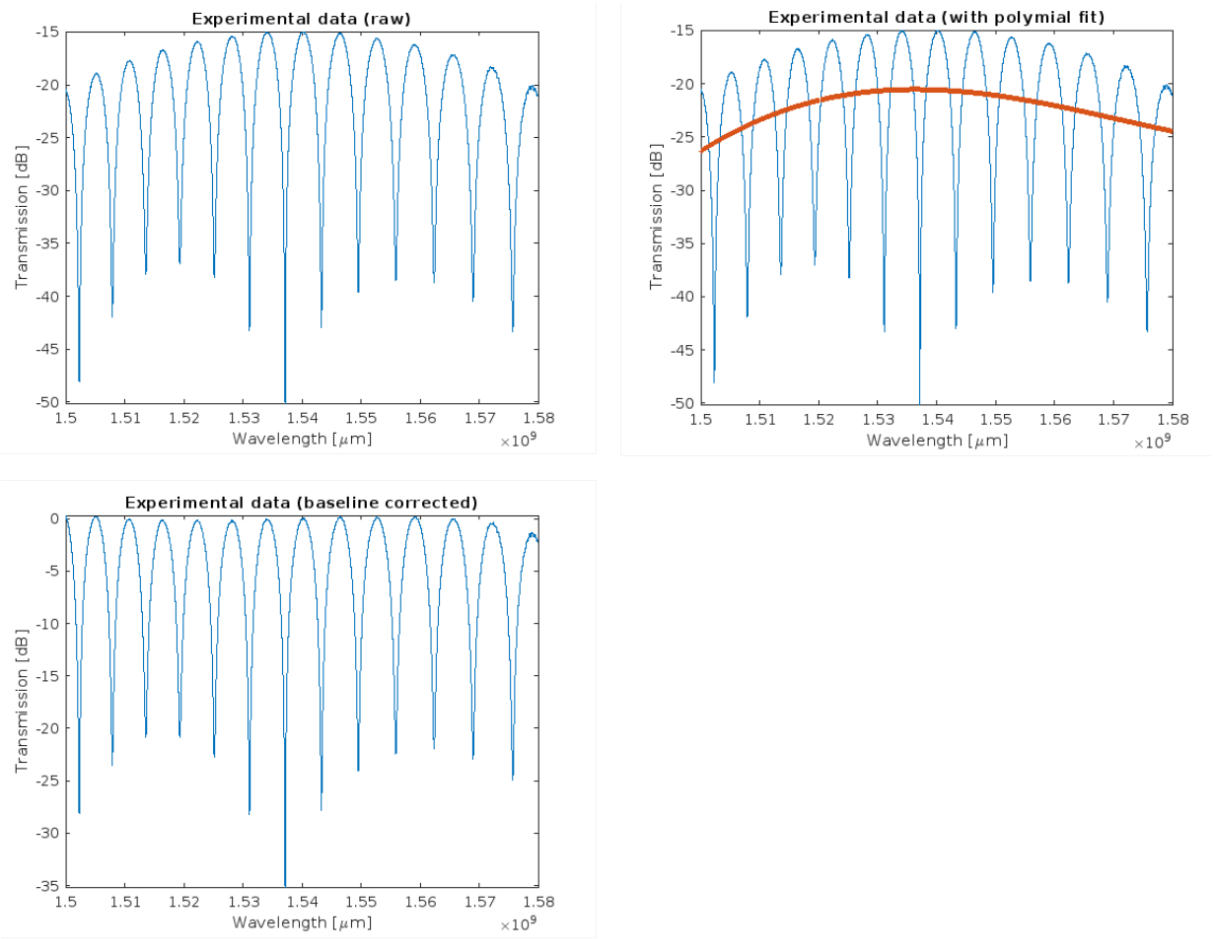

Figure 20 : TM1 Process of removing the grating couplers contribution on transmission spectrum. 1) Raw data. 2) Baseline curve in red representing grating couplers contribution. 3) Final spectrum with only MZI transmission spectrum

6 Analysis

Once curve fitting is done, we can then determine the group index by following the procedure below:

a) Correlate the experimental data with itself and get the correlation spectrum. From the correlated spectrum, estimate the FSR which can be determined from the distance between peaks.
b) From the FSR we can determine n_g, therefore we can plot the transfer function of MZI.
c) The estimated MZI transfer function is shifted vs the experimental data, thus we apply an offset to correlate the two spectra.

```
4.1880e+09
```

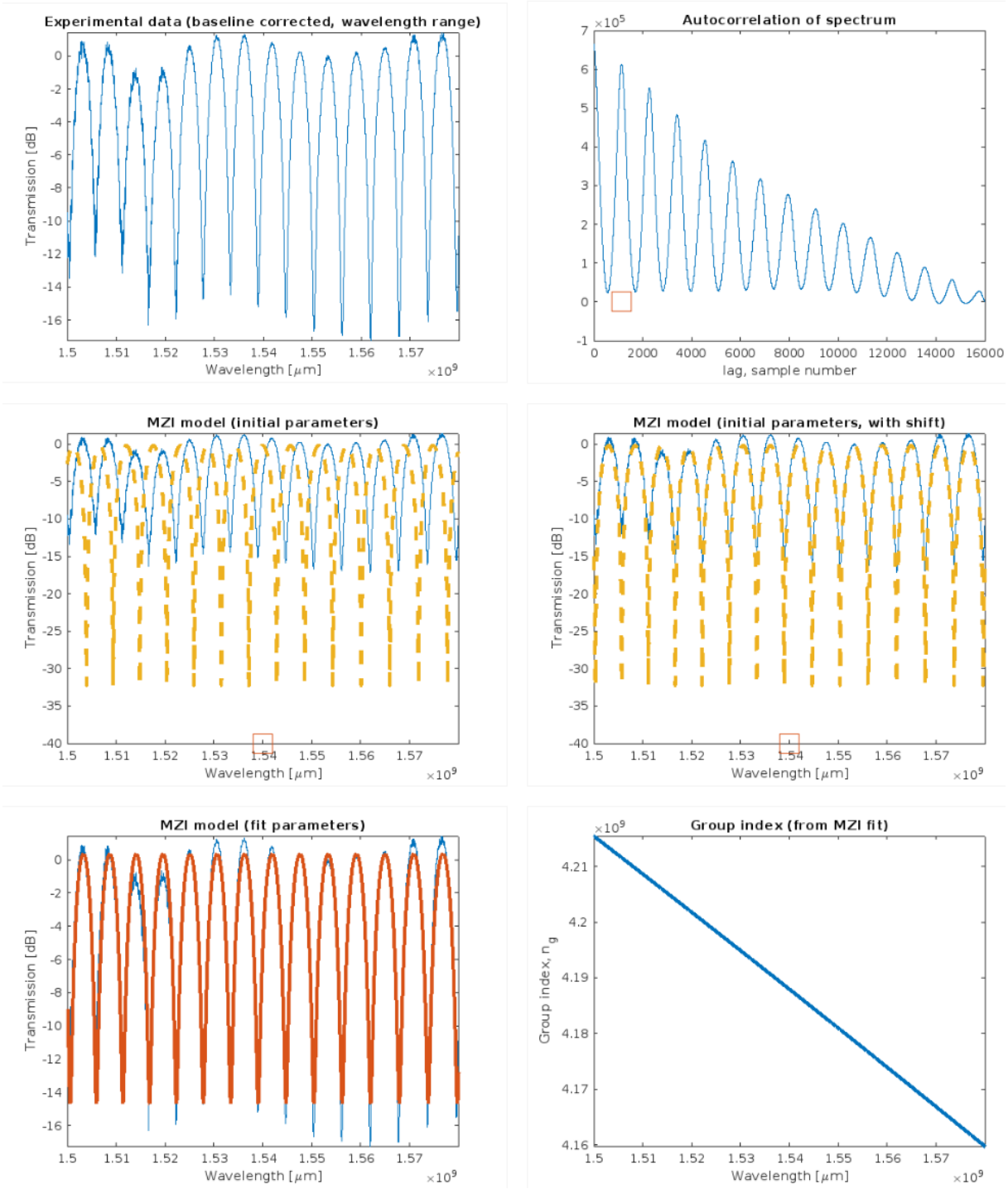

Figure 21 : TE1 MZI fitting using autocorrelation

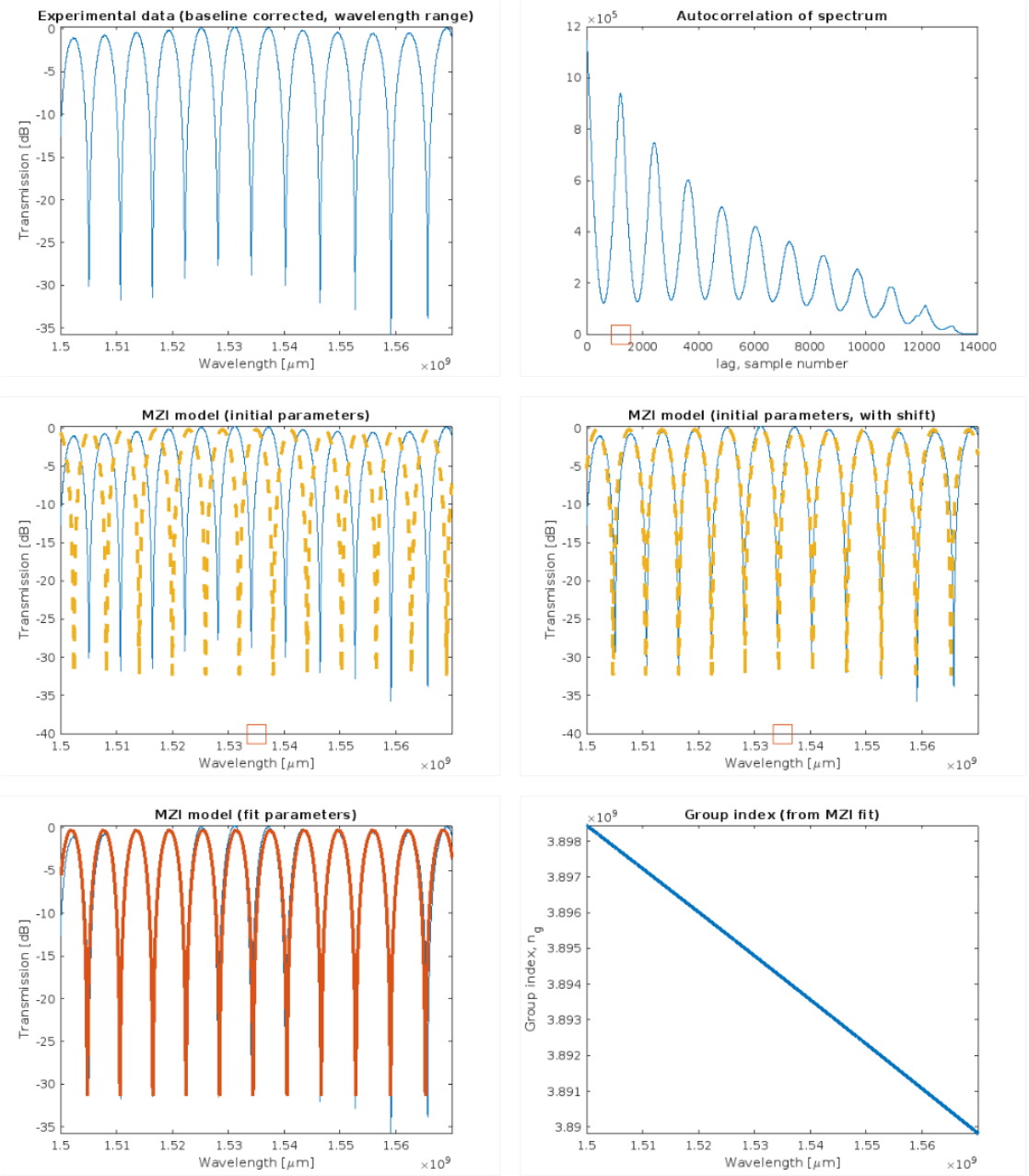

Figure 22 : TM1 MZI fitting using autocorrelation

We also want to compare the experimental results with simulation data we performed with Klayout and Lumerical.

First, we perform a Monte Carlo simulation with width variation of $\sigma = 3.9\ nm$.

On Figure 23 and Figure 24, we perform 11 simulations, and we can see the variability of the spectrum. We can see that variability on TE is higher than TM and is confirmed on Figure 25 and Figure 26 on which we can see a lower FSR and higher standard deviation than TM.

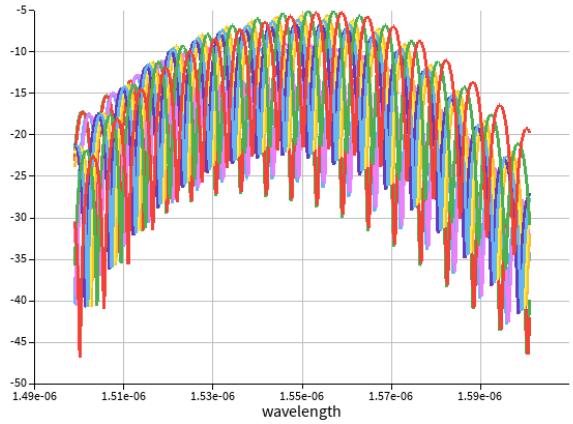

Figure 23 : transmission on TE Monte carlo simulation

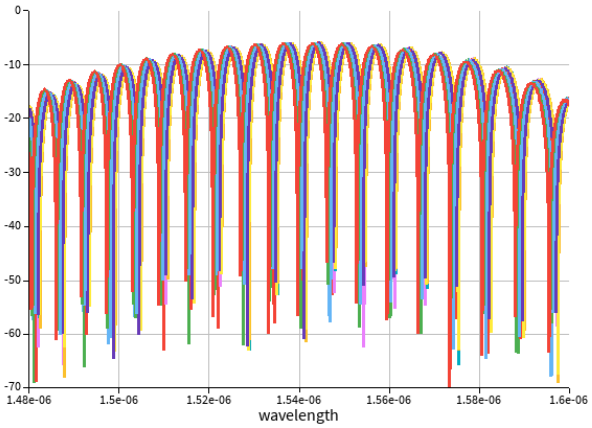

Figure 24 : transmission TE Monte carlo simulation

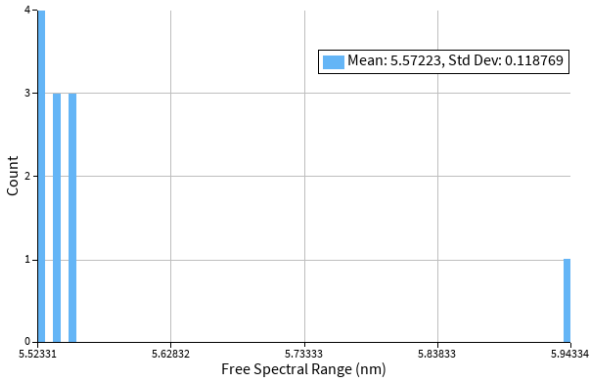

Figure 25 : FSR on TE Monte carlo simulation

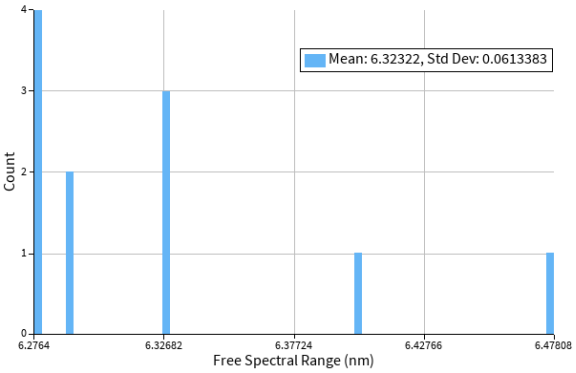

Figure 26 : FSR on TM Monte carlo simulation

Then we want to compare one of the simulations with the experimental data. On Figure 27 and Figure 28, we plot experimental data (Raw) and Simulation data (Simu) for TE and TM. Simulation data has been shifted on X and Y axis in order to reach the same scale of the experimental data. We can see that experimental data and simulation data has roughly the same periodicity but the amplitude are not well estimated specially for TE at lower wavelengths. This might be due to fabrication process, measurement parameters and probably from the grating couplers since we know that this element is highly dependent versus wavelength. We can also see that the extinction ratio of the simulation is way more optimistic than the simulation.

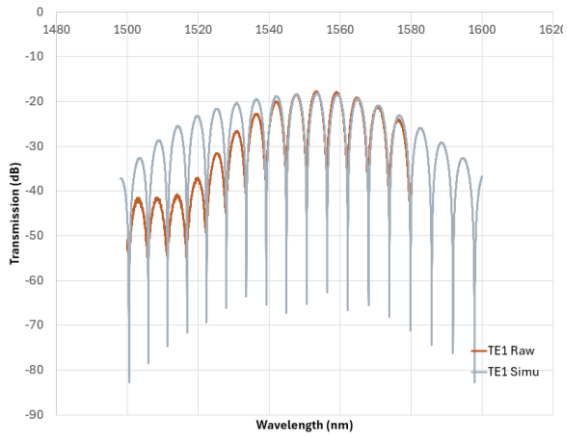

Figure 27 : TE experimental raw data vs simulation data, power offset 13 dB and wavelength offset 1 nm

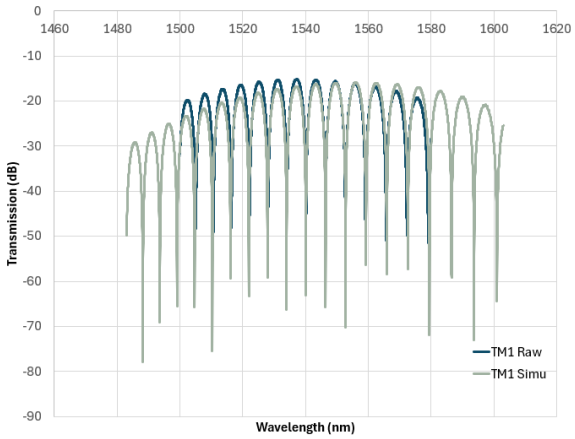

Figure 28 : TM experimental raw data vs simulation data, power offset 10 dB and wavelength offset 3 nm

If we only analyze FSR and group index in tab Table 1, as expected during simulation we can see that FSR of TE and TM are different for TE and TM even though the waveguide is squarish.

	TE Simulation	TE Experimental	TM simulation	TM Experimental
Mean FSR (nm)	5.57	5.64	6.32	6.12
ng	4.19	4.2	3.89	3.9

Table 1: FSR and ng comparison for TE and TM between simulation data and experimental data

We also want to compare quantitatively the difference between simulated data and experimental data in Table 2. We can see that the difference of FSR and ng is really low which indicates a high predictability of the SiEPIC-EBeam-PDK.

	TE Simulation - Experimental	TM Simulation - Experimental
Mean FSR (nm)	-0.07	0.2
ng	0.01	0.01

Table 2 : difference between simulation and experimental data for FSR and ng

Note that all the results we obtained previously are also repeatable for the other branch of the MZI. Thus, those data have not been shown in the report.

7 Conclusion

This first introduction to design, modelling, simulation and fabrication of PIC helps us understand the full process and major difficulties in all the process flow to get a die. During this course, I wanted to study the difficulties of having a PIC which could be insensitive to polarization and evaluate the different simulation tools that could help for design. The waveguide I designed was a 220x220 nm waveguide. We build TE and TM MZI circuits, each two times to evaluate repeatability. Experimental data shows that repeatability was not the main issue despite Monte-Carlo simulation which shows high variability especially on TE circuit. The comparison of the results between simulation and experimental data shows that wavelength dependency loss, extinction ratio,

wavelength shifts are parameters which seem difficult to predict with high precision for those circuits. Nevertheless, the correlation between the simulation and experiments on the free spectral range and group index are accurate for both TE and TM. As expected, FSR and ng are slightly different for TE and TM.

Acknowledgement

We acknowledge the edX UBCx Phot1x Silicon Photonics Design, Fabrication and Data Analysis course, which is supported by the Natural Sciences and Engineering Research Council of Canada (NSERC) Silicon Electronic-Photonic Integrated Circuits (SiEPIC) Program. The devices were fabricated by Richard Bojko at the University of Washington Washington Nanofabrication Facility, part of the National Science Foundation's National Nanotechnology Infrastructure Network (NNIN), and Cameron Horvath at Applied Nanotools, Inc. Omid Esmaeeli performed the measurements at The University of British Columbia. We acknowledge Lumerical Solutions, Inc., Mathworks, Mentor Graphics, Python, and KLayout for the design software.

Bibliographie

[1] M. H. Lukas Chrostowski, Silicon Photonics Design, Cambrigde University, 2015.

[2] L. Ansys, "https://www.lumerical.com/," [Online]. Available: https://www.lumerical.com/. [Accessed 2025].

[3] M. Caverley, " http://siepic.ubc.ca/probestation," [Online]. Available: http://siepic.ubc.ca/probestation.

[4] X. W. J. F. H. Y. W. S. R. B. N. A. F. J. L. C. Yun Wang, Focusing sub-wavelength grating couplers with low back reflections for rapid prototyping of silicon photonic circuits Optics Express Vol. 22, Issue 17, pp. 20652-20662 (2014) doi: 10.1364/OE.22.020652.

[5] U. Columbus OH, "www.plcconnections.com," PLC Connections, [Online]. Available: www.plcconnections.com.

[6] http://mapleleafphotonics.com, "Maple Leaf Photonics," Seattle WA, USA. [Online].

[7] Lukas Chrostowski and Michael Hochberg, Silicon Photonics Design: From Devices to Systems, Cambridge University Press, 2015.